arXiv:1209.2837v1 [cond-mat.soft] 13 Sep 2012

Capillary-like Fluctuations of a Solid-Liquid Interface in a Non-Cohesive Granular System

Li-Hua Luu,* Nicolás Mujica, and Rodrigo Soto
Departamento de Física, Facultad de Ciencias Físicas y Matemáticas
Universidad de Chile, Avenida Blanco Encalada 2008, Santiago, Chile
(Dated: September 14, 2012)

One of the most noticeable collective motion of non-cohesive granular matter is clustering under certain conditions. In particular, when a quasi-two-dimensional monolayer of mono-disperse non-cohesive particles is vertically vibrated, a solid-liquid-like transition occurs when the driving amplitude exceeds a critical value. Here, the physical mechanism underlying particle clustering relies on the strong interactions mediated by grain collisions, rather than on grain-grain cohesive forces. In average, the solid cluster resembles a drop, with a striking circular shape. We experimentally investigate the solid-liquid interface fluctuations, which are characterized through the static and dynamic correlation functions in the Fourier space. These fluctuations turn out to be well described by the capillary wave theory, which allows us to measure the grain-boundary surface tension and mobility once the granular "thermal" kinetic energy is determined. Furthermore, both quantities are consistent with a simple order of magnitude estimation considering the characteristic energy, length and time scales, which is very similar to what can be done for atomic systems.

PACS numbers: 05.40.-a 45.70.-n, 68.08.-p

Granular matter, composed by a collection of macroscopic particles that interact via dissipative contacts, is fundamentally out of equilibrium. When energy is injected into an athermal granular system, constant grain rearrangements are induced and accompanied by friction and inelastic particle collisions. In particular, dense granular materials exhibit a large variety of interesting phenomena, under static conditions or in a dynamical state. Notorious examples are granular piles, avalanches, segregation, pattern formation, granular phase coexistence and jamming [1–3]. Since few decades, extensive research has been conducted on granular phase transitions. One case of interest is the solid-liquid coexistence during an avalanche, where the characterization of the two-phase interface allows the study of the granular rheology [3]. Another system of interest is vibrated granular layers that reveal Faraday waves patterns that are preceded by a solid-to-liquid transition [4, 5].

Dry granular systems are usually considered to have no surface tension. However, several recent studies show that non-cohesive or very weakly cohesive granular materials develop phenomena driven by surface tension, which can be low but not zero. Some remarkable examples are the Rayleigh-Taylor-like instability in tapped powders [6] and the interfacial instabilities in falling granular streams, in air [7] and vacuum [8]. In other cases, granular systems are shown to behave as a zero-surface-tension liquid, as for particle sheets (analog to "water bells") created by a granular jet impacting a target [9] and fingering in a granular Hele-Shaw system [10]. The point is to understand how capillary-like features can emerge out of collections of particles that are known to be almost or completely non-cohesive. In some cases, an hydrodynamic derivation conducting a zero-surface-tension limit succeed in describing the observations [9, 10]; in other situations, a low effective surface tension depending on the granular system dynamics is estimated, either considering the flow of interstitial air [6, 7] or nano-Newton cohesion forces in the case of very low external forcing [8].

Here, we experimentally investigate a granular system composed by non-cohesive mono-disperse grains that are confined in quasi-2D geometry. This geometry allows the characterization of both individual grain motion and collective behavior. When such system is vertically vibrated, it can present a transition from a completely fluidized state to the coexistence of a liquid state with solid (ordered) clusters [11–13]. It has been recently shown that such coexistence is triggered by a negative compressibility, as observed in a similar gas-liquid van der Waals granular transition [14, 15], and that density waves propagate in the system [12]. In our previous work [13] we show that depending on the vertical height and filling density the transition can be of either first or second order type. For both cases density fluctuations do not show strong variations at the transition, but local order varies strongly, either abruptly or continuously respectively, with a critical-like behavior in the second case.

In this Letter, we stand in the stationary regime of phase coexistence in the case where the transition is continuous. Above a critical driving amplitude a unique solid cluster is observed. We focus on the liquid-solid-like interface characterization. In average, the granular cluster exhibits a striking circular shape, like a drop, modulated by important grain-boundary fluctuations (see Fig. 1). Our approach is similar to the one proposed in [7], consisting in an analogy with condensed matter at molecular scale where thermal agitation induces capillary waves that deform an interface. Thus, we aim to discuss to what extent it is valid to use some concepts of kinetic theory to describe our macroscopic athermal granular matter,

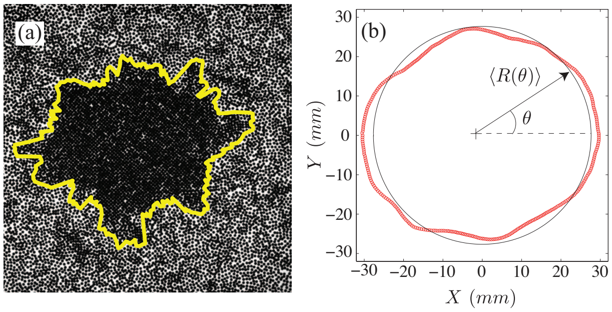

FIG. 1. (color online) (a) Typical image showing a solid-like cluster in coexistence with a liquid-like phase. The continuous line shows the grain-boundary detection. (b) Time averaged solid-liquid-like interface $\langle R(\theta)\rangle$ from about 7000 images. The continuous line shows the circle of radius $R_0 = 27.7$ mm obtained from angle averaging $\langle R(\theta)\rangle$.

in order to express the strong interactions mediated by grain collisions in terms of effective surface tension and grain-boundary mobility formulations.

The experimental setup is the same one reported previously [13, 16]. It consists of a container confining a layer of $N = 11504$ stainless steel spherical particles in a shallow box with transverse dimensions $L_x = L_y = 100d$ and height $L_z = 1.94d \pm 0.02d$, where $d = 1$ mm is the particle diameter (configuration 2 of our previous study [13]). The top and bottom glass plates of the cell are directly in contact with the particles and the side walls. Particles are illuminated from below with an array of light emitting diodes and a high speed video camera enables particle detection and tracking. The surface coverage is defined by the filling fraction $\phi = N\pi d^2/4L^2 = 0.904$. We submit the system to vertical sinusoidal vibrations, with displacement $z(t) = A\sin(\omega t)$, where A is the vibration amplitude. Its motion is controlled with a piezoelectric accelerometer. Special care is devoted to the control of the horizontality. For this configuration, a second-order solid-liquid-like transition occurs when the dimensionless acceleration $\Gamma = A\omega^2/g$ reaches a critical value $\Gamma_c \approx 5.1$ ($f = 2\pi/\omega = 80$ Hz). In the framework of the solid cluster's characterization, the present study is done at $\Gamma = 6.30 \pm 0.03$ and $f = 80$ Hz.

Figure 1 displays typical results of the interface detection. To distinguish the liquid phase from the solid phase, we use a Voronoï cell's area criterion. For each particle, if its Voronoï area is lower than a critical value determined empirically [13], it is considered in the solid phase; otherwise, its in the liquid phase. Then, using coarse-grained polar coordinates ($\Delta\theta = 1°$), we detect 360 interfacial particles in each image. The origin of the polar coordinate system is fixed at the time-averaged center of mass of the solid-like particles. We observe that the time-averaged interface exhibits a circular shape with a mean radius of $R_0/d = 27.7 \pm 1.5$.

In this study, we consider a curve-driven interface behavior for the steady state cluster. In condensed matter, from the classical solid to liquid phases, any interface is microscopically rough due to the competition between thermal energy and minimization of surface area [17]. The grain-boundary evolution is involved in processes such as crystallization in solution [18] or dendritic solidification [19], and controls structural and mechanical properties of many materials [20]. The first interfacial parameter studied is the grain-boundary stiffness, $\tilde{\gamma} = \gamma + \gamma''$, where γ is the surface tension and γ'' its second derivative with respect to the spatial coordinate. In our case, we make a small slope approximation for the interface, $\tilde{\gamma} \approx \gamma$. The second interfacial parameter is the grain-boundary mobility M, defined by $V = M\gamma\kappa$, with V the grain-boundary velocity and κ the interface curvature. Inspired by theoretical and numerical studies on interfacial properties of molecular systems [21, 22], and on an experimental study of colloidal crystals [23], we attempt to obtain these physical quantities applying a capillary wave description.

In analogy to the capillary theory in condensed matter, we will assume that there is a functional, analog to the free energy that is minimized in the stationary state and allows to obtain the dynamics close to the stationary state. This assumption, although no fully justified in non-equilibrium systems, is made for simplicity and verified *a posteriori* as its predictions are consistent with the experimental results. To follow the analogy with equilibrium systems, this functional will be refered as *non-equilibrium free energy*.

First, we consider the interface contribution to the non-equilibrium free energy E_γ. In two dimensions, it is related to the cluster's arc length and by an effective surface tension γ such as $E_\gamma = \gamma \int_0^{2\pi} \sqrt{R^2 + (\partial_\theta R)^2}\, d\theta$, with $R(\theta, t)$ the cluster's radius. Because of the system finite size, which implies a finite number of particles and a finite stationary radius, an additional mass term has to be added to obtain the total non-equilibrium free energy (for details see [24]). The radius fluctuations are defined as $\delta R(\theta, t) = R(\theta, t) - R_0$, where R_0 is the mean radius in time and in space. Its Fourier representation is

$$\delta R(\theta, t) = \sum_{m=-\infty}^{\infty} \widetilde{\delta R}_m(t) \exp(im\theta). \qquad (1)$$

For small radial fluctuations, it is direct to show [24] that energy fluctuations obey

$$\delta E = \frac{\pi\lambda}{R_0}|\widetilde{\delta R}_0|^2 + \frac{\pi\nu}{R_0}\left(|\widetilde{\delta R}_1|^2 + |\widetilde{\delta R}_{-1}|^2\right) \qquad (2)$$
$$+\frac{\pi\gamma}{R_0}\sum_{|m|\geq 2}|\widetilde{\delta R}_m|^2(m^2-1),$$

where the first term corresponds to changes in size, the second to changes in position, which exists because the

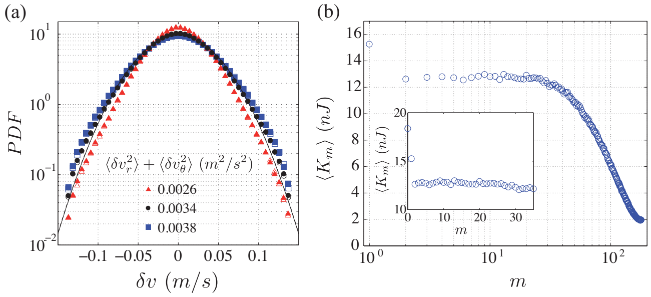

FIG. 2. (color online) (a) The probability density function (PDF) of velocity fluctuations (open and solid symbols for radial and tangential components respectively): in the liquid-like domain (■), for the grain-boundary particles (●) and in the solid-like domain (▲). The continuous line is a Gaussian fit to the PDF of the grain-boundary particle velocity fluctuations. (b) Average horizontal kinetic energy spectrum, $\langle K_m \rangle$ versus m, in semi-log scale. The inset shows the linear plot for $m = 0, ..., 35$.

translational symmetry is not perfect in the experiment and the cluster has a tendency to remain in the center of the box, and the third term corresponds to changes of the cluster's shape. Only the last term is related to the surface tension γ and the other two introduce new coefficients, ν and λ, that should be measured as well. From here, the static power spectrum is obtained

$$\langle |\widetilde{\delta R}_0|^2 \rangle = \frac{\langle K_0 \rangle R_0}{\pi \lambda}, \quad \langle |\widetilde{\delta R}_{\pm 1}|^2 \rangle = \frac{\langle K_1 \rangle R_0}{\pi \nu}, \qquad (3)$$

$$\langle |\widetilde{\delta R}_{|m| \geqslant 2}|^2 \rangle = \frac{\langle K_{|m| \geqslant 2} \rangle R_0}{\pi \gamma (m^2 - 1)}. \qquad (4)$$

where $\langle\,\rangle$ denotes time average. The quantity $\langle K_m \rangle = \frac{1}{2} N_p m_p \langle |\tilde{v}_m^x|^2 + |\tilde{v}_m^y|^2 \rangle$ is the average horizontal kinetic energy per mode, where N_p is the number of particles at the solid-liquid interface, $m_\mathrm{p} = 4.45 \pm 0.01$ mg is the particle mass and $\tilde{v}_m^x$ and $\tilde{v}_m^y$ are the interface particle's velocity Fourier components [24]. $\langle K_m \rangle$ is the equivalent of the thermal energy $k_B T/2$ per mode at equilibrium. Although related, $\langle K_m \rangle$ is not equal to the usually defined granular temperature $T_g = \frac{1}{2} m_\mathrm{p} \vec{v}^{\,2}$, because the number of active modes is not $2N_p$.

Figure 2a displays the probability density function (PDF) of particle velocities in the liquid (l) and solid (s) phases, as well as for the particles at the boundary (b). The PDFs are almost Gaussian, with deviations for large fluctuations. They are centered on zero and we verify isotropy between the horizontal velocity components. The granular temperature T_g, obtained from the variance of the velocity distributions, is not uniform. Indeed, because of the collisional and dissipative nature of particle interactions, higher particle volume fraction implies higher dissipation and lower T_g. As expected, we obtain $T_g^\mathrm{l} > T_g^\mathrm{b} > T_g^\mathrm{s}$. In Fig. 2b we present the average horizontal kinetic energy spectrum, $\langle K_m \rangle$ versus m. We observe energy equipartition between $m = 2$ and $m \approx 30$, with an average value $K_\mathrm{eq} = 12.7 \pm 0.2$ nJ. For comparison, the boundary granular temperature $T_g^\mathrm{b} \approx 7.5$ nJ. The two lowest modes have larger energy, $\langle K_0 \rangle = 18.4 \pm 11.3$ nJ and $\langle K_1 \rangle = 15.3 \pm 7.2$ nJ, and the energy components decrease continuously to zero for $m > 30$.

Figure 3a shows a very satisfactory agreement for the experimental power spectrum (4) with a $1/(m^2 - 1)$ tendency, within a physically relevant range for the wavenumber $m = 6 - 35$, corresponding to wavelengths $2\pi R_o/m \approx 5d - 29d$. Fitting Eqn. (4) to the experimental data gives an effective surface tension $\gamma = 4.6 \pm 0.3$ μN in two-dimensions, and using L_z as the third dimension, we get $\gamma_\mathrm{3D} \equiv \gamma / L_z = 2.4 \pm 0.2$ mN/m. Additionally, λ and ν can be measured through the components $m = 0$ and $m = 1$ of $\langle |\widetilde{\delta R}_m|^2 \rangle$ and $\langle K_m \rangle$, obtaining $\lambda = 0.30 \pm 0.28$ mN, and $\nu = 0.23 \pm 0.18$ mN.

For comparison, our measured surface tension γ_3D is about 30 times smaller than pure water's surface tension, but it is much larger than the surface tension 0.1 μN/m estimated for a freely falling dry granular material [8]. In fact, this latter work demonstrates that nano-Newton cohesive interaction forces, measured by AFM, are responsible for the surface tension. In our case, the physical mechanism is not originated by grain-grain cohesion, but from dissipative collisions between particles. Actually, the effective surface tension of our system can be estimated as $\gamma \sim T_g^\mathrm{b}/d \approx 7.5$ μN, which implies $\gamma_\mathrm{3D} \sim T_g^\mathrm{b}/(d L_z) \approx 4$ mN/m. This result is consistent with the scaling found in a recent numerical study on 3D crystallization of hard spheres, where the fluid-solid surface tension is $\gamma_\mathrm{3D} \sim k_B T/d^2$ [25].

From the definition of the grain-boundary mobility M, it is direct to show that each mode obeys a Langevin equation (see details in [24]):

$$\frac{\partial \widetilde{\delta R}_m}{\partial t} = -\frac{1}{\tau_m} \widetilde{\delta R}_m + M \eta_m(t), \qquad (5)$$

where $\tau_m = R_0^2/[M\gamma(m^2 - 1)]$ for $|m| \geqslant 2$, and $\tau_0 = R_0^2/(M\lambda)$ and $\tau_{\pm 1} = R_0^2/(M\nu)$ for $m = 0$ and $m = \pm 1$ respectively, are the relaxation times and $\eta_m(t)$ are the Fourier modes of the noise term $\eta(\theta, t)$ in real space, which is assumed to be delta correlated. From here, the following expression for the dynamic correlation function in Fourier space is derived:

$$\langle \widetilde{\delta R}_m(t) \widetilde{\delta R}_m^*(0) \rangle = \langle |\widetilde{\delta R}_m|^2 \rangle e^{-t/\tau_m}. \qquad (6)$$

Figure 3b displays a good agreement for the predicted exponential decay. The data for $t > 0.2$ s and for $m > 18$ are very noisy and not represented here. On one hand, the intercept of the exponential decay for $t = 0$ should be equal to $\log(\langle |\widetilde{\delta R}_m|^2 \rangle)$, and so vary linearly with $\log(m^2 - 1)$. Although it does show this behavior, it is

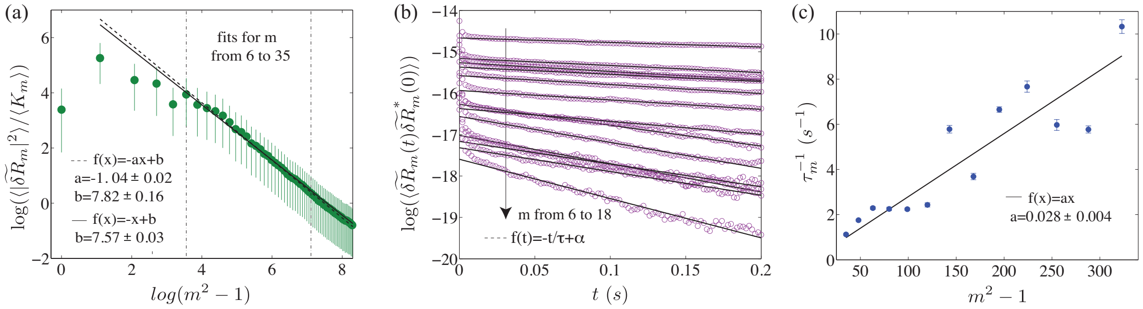

FIG. 3. (color online) (a) Static analysis using ≈ 7000 images. The average static power spectrum of the radius fluctuations $\langle|\widetilde{\delta R}_m|^2\rangle$, over the average horizontal kinetic energy spectrum $\langle K_m\rangle$, as a function of m^2-1 in log-log scale. (b-c) Dynamic correlation function analysis. (b) Two-time correlation function $\langle\widetilde{\delta R}_m(t)\widetilde{\delta R}_m^*(0)\rangle$ for several m, which show exponential decay. (c) Decay time τ_m^{-1} versus (m^2-1). The continuous line shows the linear law fit. The error bars represent the dispersion over two successive experiments.

systematically lower than $\log(\langle|\widetilde{\delta R}_m(0)|^2\rangle)$. When computing this last quantity, we observe that the $1/(m^2-1)$ dependency is consistent. Fitting Eqn. (4) gives the same result for γ than previously determined, $\gamma = 4.3\pm0.3\ \mu$N. On the other hand, τ_m^{-1} increases linearly with (m^2-1), as shown un Fig. 3c. Putting numbers, we obtain the grain-boundary mobility $M = 5.0\pm0.8$ m^{3}J^{-1}s^{-1}. We remark that for an atomic system simulation [21], the mobility in two-dimensions scales as $M \sim l_c^3/(k_BTt_c)$, with k_BT the thermal agitation, l_c and t_c characteristic length and time respectively. In our case, considering $k_BT = T_g^{\mathrm{b}}$, $l_c \sim d$ and $t_c \sim d/\sqrt{\langle\delta\vec{v}_{\mathrm{b}}^2\rangle}$, yields the same order of magnitude for the mobility $M \approx 8$ m^{3}J^{-1}s^{-1}.

Another way to obtain the grain-boundary parameters λ, ν, and M is from a square-displacement analysis for $m=0$ and $m=1$. Indeed, from Eq. (5), the mean square displacement for each mode is

$$\langle|\Delta R_{0,1}|^2\rangle = \frac{2M\langle K_{0,1}\rangle\tau_{0,1}}{\pi R_0}\left(1-e^{-t/\tau_{0,1}}\right), \qquad (7)$$

where $\Delta R_{0,1} = \widetilde{\delta R}_{0,1}(t) - \widetilde{\delta R}_{0,1}(0)$. For short times $t \ll \tau_{0,1}$, a diffusive behavior is expected for each mode, $\langle|\Delta R_{0,1}|^2\rangle \approx 2D_{0,1}t$, with $D_{0,1} = M\langle K_{0,1}\rangle/(\pi R_0)$, which is the analog of the fluctuation-dissipation relation used in atomic simulations for flat geometries [21, 22].

Figure 4 displays $\langle|\Delta R_m|^2\rangle - c_m$ as a function of time for $m=0$ and $m=1$. Here, c_m is a parameter obtained from the fit $\langle|\Delta R_m|^2\rangle = A_m[1-\exp(-t/\tau_m)]+c_m$, which reflects the fact that the Langevin equation for each mode does not describe the first ballistic regime for very short times. The continuous lines represent the fit for each mode, showing a very good agreement. The predicted saturation is observed for long times, and the intermediate diffusive regime is also manifested. From the fitted values of A_m and τ_m we obtain $\lambda = 0.7\pm0.4$ mN, $\nu = 0.4\pm0.2$ mN, $M_0 = 1.3\pm0.8$ m^{3}J^{-1}s^{-1}, and $M_1 = 2.5\pm1.2$ m^{3}J^{-1}s^{-1}. Both mobilities should in principle be equal, and the same as measured for larger m. The agreement between these values and those measured from the static and dynamic correlation functions seems good enough considering the large errors in each quantity.

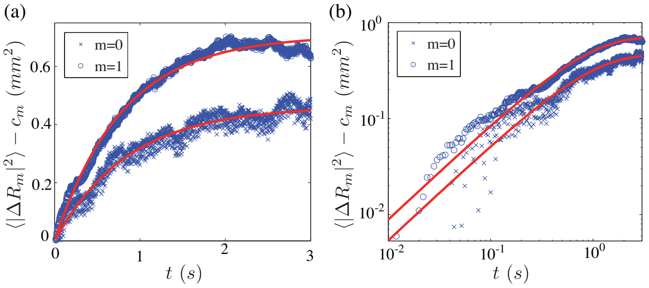

FIG. 4. (color online) Mean square displacement analysis for $m=0$ and $m=1$, in linear (a) and log-log scale (b). Each curve is the result of the average of two realizations. The solid lines correspond to fits $\langle|\Delta R_m|^2\rangle = A_m[1-\exp(-t/\tau_m)]+c_m$.

To conclude, we have demonstrated that the liquid-solid-like interface in a quasi-2D vibrated granular system can be characterized by grain-boundary's parameters such as surface tension and interfacial mobility. Both quantities are consistent with a simple order of magnitude estimation considering the characteristic energy, length and time scales, which is very similar to what can be done for atomic systems. The scaling of the effective surface tension with the granular temperature T_g^{b} suggests that the particles' kinetic energy plays the role of the cohesive energy that originates capillary-like phenomenon in molecular liquids. It would be interesting to relate the particle kinetic energy to a collisional pressure in each phase. By doing so, we could handle the surface tension concept by thinking in terms of pressure difference, as defined by the hydrodynamic law of Laplace. This perspective would allow to couple a particle's scale study (e.g. by accounting for collisions, cross section and contact duration determination) to a macroscopic description and would arise the question of particle pressure in granular media, well-known for homogeneous gas-fluidized bed [26], but still open for high density granular flows.

We thank G. Castillo and F. Barra for valuable technical help and discussions. This research is supported by Fondecyt Grants No. 3120172 (L.-H.L), No. 1120211 (N.M.) and No. 1100100 (R.S.), and Anillo grant ACT 127.

---

* Corresponding author: luulihua@yahoo.fr

[1] H.M. Jeager, S.R. Nagel and R.P. Behringer, Rev. Mod. Phys. **68**, 1259 (1996).

[2] I.S. Aranson and L.S. Tsimring, Rev. of Mod. Phys. **78**, 641 (2006).

[3] O. Pouliquen and Y. Forterre, Annu. Rev. Fluid Mech. **40**, 1 (2008).

[4] P.B. Umbanhowar, F. Melo and H.L. Swinney, Nature **382**, 793 (1996).

[5] N. Mujica and F. Melo, Phys. Rev. Lett. **80**, 5121 (1998).

[6] J. Duran, Phys. Rev. Lett. **87**, 254301 (2001).

[7] Y. Amarouchene, J.F. Boudet, and H. Kellay, Phys. Rev. Lett. **100**, 218001 (2008).

[8] J.R. Royer *et al.*, Nature **459**, 1110-1113 (2009).

[9] X. Cheng, G. Varas, D. Citron, H.M. Jaeger, S.R. Nagel, Phys. Rev. Lett. **99**, 188001 (2007).

[10] X. Cheng *et al.*, Nature Phys. **4**, 234-237 (2008).

[11] A. Prevost, P. Melby, D. A. Egolf, and J. S. Urbach, Phys. Rev. E **70**, 050301(R) (2004).

[12] M.G. Clerc *et al.*, Nature Physics **4**, 249 (2008).

[13] G. Castillo, N. Mujica and R. Soto, Phys. Rev. Lett. **109**, 095701 (2012).

[14] M. Argentina, M.G. Clerc, R. Soto, Phys. Rev. Lett. **89**, 044301 (2002).

[15] C. Cartes, M.G. Clerc and R. Soto, Phys. Rev. E **70**, 031302 (2004).

[16] N. Rivas *et al.*, Phys. Rev. Lett. **106**, 088001 (2011).

[17] J.M.Howe, Interfaces in Materials (Wiley, New York, 1997).

[18] D. Mangin *et al.*, Organic Process Research & Development **13**, 1241-1253 (2009).

[19] J.J. Hoyt *et al.*, Materials Science and Engineering R **41**, 121-163 (2003).

[20] S. Yip, Nature **391**, 532-533 (1998).

[21] Z.T. Trautt, M. Upmanyu and A. Karma, Science **314**, 632-635 (2006).

[22] J.J. Hoyt *et al.*, Mathematics and Computers in Simulation **80**, 1382-1392 (2010).

[23] T.O.E. Skinner, D.G.A.L. Aarts, and R.P.A. Dullens, Phys. Rev. Lett. **105**, 168301 (2010).

[24] See Supplemental Material at http://link.aps.org/sup-plemental/XX.XXXX/PhysRevLettXXX.X for the deduction of the non-equilibrium free energy, the analysis of the granular temperature and energy per mode, a description of the Langevin dynamics, and the error analysis.

[25] L.A. Fernández, V. Martin-Mayor, B. Seoane, and P. Verrocchio, Phys. Rev. Lett. **108**, 165701 (2012).

[26] G.K. Batchelor, J. Fluids Mech. **193**, 75-110 (1988).